Hyperelasticity governs dynamic fracture at a critical length scale

Markus J. Buehler[1]*, Farid F. Abraham[2]* & Huajian Gao[1]*

[1]*Max Planck Institute for Metals Research, Heisenbergstrasse 3, 70569 Stuttgart, Germany*
[2]*IBM Research Division, Almaden Research Center, 650 Harry Road, San Jose, California 95120, USA*

* These authors contributed equally to this work

The elasticity of a solid can vary depending on its state of deformation. For example, metals will soften and polymers may stiffen as they are deformed to levels approaching failure. It is only when the deformation is infinitesimally small that elastic moduli can be considered constant, and hence the elasticity linear. Yet, many existing theories model fracture using linear elasticity, despite the fact that materials will experience extreme deformations at crack tips. Here we show by large-scale atomistic simulations that the elastic behaviour observed at large strains—hyperelasticity—can play a governing role in the dynamics of fracture, and that linear theory is incapable of fully capturing all fracture phenomena. We introduce the concept of a characteristic length scale for the energy flux near the crack tip, and demonstrate that the local hyperelastic wave speed governs the crack speed when the hyperelastic zone approaches this energy length scale.

Why and how cracks spread in brittle materials is of essential interest to numerous scientific disciplines and technological applications, and a theoretical understanding is essential for many engineering applications. We show by large-scale atomistic simulation that hyperelasticity, the elasticity of large strains, can play a governing role in the dynamics of brittle fracture. This is in contrast to many existing theories of dynamic fracture where the linear elastic behaviour of solids is assumed to be sufficient to predict materials failure[1–3]. Real solids have elastic properties that are significantly different for small and for large deformations.

Many phenomena associated with rapidly propagating cracks are not thoroughly understood. Some experimental work[4,5] as well as many computer simulations[6–8] have shown a significantly reduced crack propagation speed in comparison with the predictions by the theory. In contrast, other experiments indicated that over 90% of the Rayleigh wave speed can be achieved[9–15]. Such discrepancies between theories, experiment and simulations cannot always be attributed to the fact that real solids have all sorts of imperfections such as grain boundaries and microcracks (either pre-existing or created during the crack propagation), because similar discrepancies also appear in molecular-dynamics simulations of cracks travelling in perfect atomic lattices.

Gao[16,17] and Abraham[7,18,19] have independently proposed that hyperelastic effects at the crack tip may play an important role in the dynamics of fracture. Their suggestions have been used to help interpret phenomena related to crack branching and dynamic crack tip instability, as well as explaining the significantly lower maximum crack propagation speed observed in some experiments and many computer simulations. However, it is not generally accepted that hyperelasticity should play a significant role in dynamic fracture. One reason for this belief stems from the fact that the zone of large deformation in a loaded body with a crack is highly confined to the crack tip, so that the region where linear elastic theory does not hold is extremely small compared to the extensions of the specimen[1,2].

In this study, we use large-scale molecular-dynamics simulations[19–24] in conjunction with continuum mechanics concepts[1,2] to prove that hyperelasticity can be crucial for understanding dynamic fracture. Our study shows that local hyperelasticity around the crack tip can significantly influence the limiting speed of cracks by enhancing or reducing local energy flow. This is true even if the zone of hyperelasticity is small compared to the specimen dimensions. The hyperelastic theory completely changes the concept of the maximum crack velocity in the classical theories. For example, the classical theories clearly predict that mode I cracks are limited by Rayleigh wave speed and mode II cracks are limited by longitudinal wave speed. In contrast, both super-Rayleigh mode I and supersonic mode II cracks are allowed by hyperelasticity and have been seen in computer simulations[23,25]. In our simulations, we find that there exists a characteristic length scale associated with energy flow near the crack tip such that hyperelasticity completely dominates crack dynamics if the size of the hyperelastic region approaches this characteristic length. In earlier simulations[23,25], a nonlinear interatomic stiffening was assumed, and there was no sharp distinction between the linear and nonlinear elastic regimes for the stretched solid. In contrast, our model is based on a biharmonic potential composed of two spring constants, one associated with small deformations and the other associated with large deformations. This serves as a simplistic model material for hyperelasticity, allowing us to investigate the generic features of hyperelasticity common to a large class of real materials.

Modelling

We consider propagation of a crack in a two-dimensional simulation geometry shown in Fig. 1. The slab size is given by l_x and l_y.

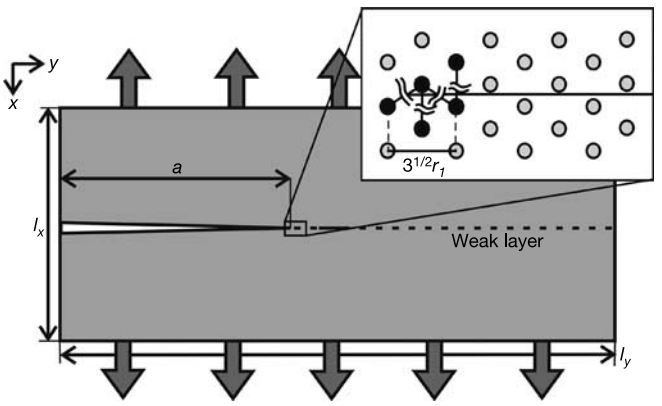

Figure 1 The simulation geometry with the lattice orientation and the weak layer. The crack propagates in the *y* direction, and the slab is loaded in mode I in the *x* direction. A slit of length $a = 200$ serves as an initial crack.

The crack propagates in the y direction, and its extension is denoted by a. The crack propagates in a triangular hexagonal lattice with nearest-neighbour distance $r_1 = 2^{1/6} \approx 1.12246$ along the crystal orientation shown in Fig. 1. To avoid crack branching, a weak fracture layer is introduced by assuming that atomic bonds across the prospective crack path snap at a critical atomic snapping distance r_{break} while those in the rest of the slab never break. The snapping distance can be used to adjust the fracture surface energy γ.

We adopt a biharmonic, interatomic potential composed of two spring constants $k_1 = 36/\sqrt[3]{2} \approx 28.57$ and $k_2 = 2k_1$ (all quantities given are in dimensionless units). We consider two 'model materials', one with elastic stiffening and the other with elastic softening behaviour. In the elastic stiffening system, the spring constant k_1 is associated with small perturbations from the equilibrium distance r_1, and the second spring constant k_2 is associated with large bond stretching for $r > r_{on}$. The role of k_1 and k_2 is reversed in the elastic softening system ($k_1 = 2k_2$, and $k_2 = 36/\sqrt[3]{2}$). Purely harmonic systems are obtained if r_{on} is chosen to be larger than r_{break}.

Poisson's ratio is found to be approximately independent of strain and around $\nu \approx 0.33$ for all potentials. In the stiffening system, the small deformation (up to about 0.5% of strain) Young's modulus is $E_1 = 33$ with shear modulus $\mu = 12.4$, and the large deformations tangent Young's modulus is $E_2 = 66$ with shear modulus $\mu_2 = 24.8$. The values are reversed for the softening system where the small deformation Young's modulus is $E_1 = 66$, and the large deformation tangent Young's modulus is $E_2 = 33$. The two-dimensional sheet of atoms behaves as an isotropic plane stress sheet at small deformation.

There are three distinct wave velocities in elastic solids: the longitudinal wave speed $c_l = \sqrt{3\mu/\rho}$, the shear wave speed $c_s = \sqrt{\mu/\rho}$ and the Rayleigh wave speed $c_r \approx 0.9225 c_s$, with the density $\rho = 2/\sqrt{3}/\sqrt[3]{2} \approx 0.9165$ for atomic mass $m = 1$. It follows from the choice of $k_2 = 2k_1$ that there is a ratio of $\sqrt{2}$ between small and large deformation wave speed.

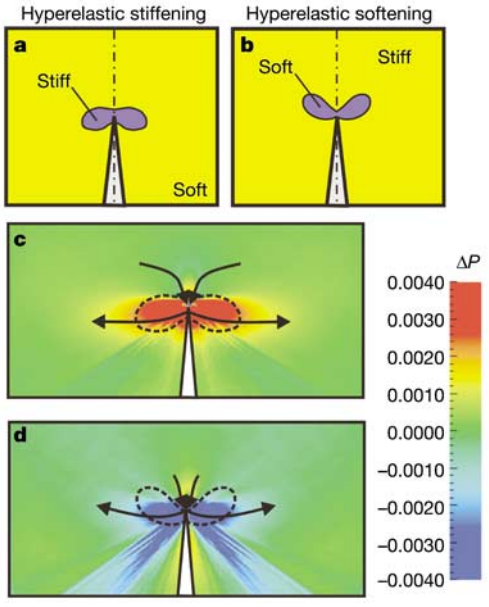

Figure 2 Hyperelastic zone and the associated change in energy flow near the crack tip. **a**, **b**, The hyperelastic zones for the bilinear stiffening system and the softening system, respectively. **c**, **d**, The associated change of energy flow ΔP in the stiffening and softening systems. The local hyperelastic zone is indicated in purple in **a** and **b** and by a dotted line in **c** and **d**. Plots **a** and **b** show a section of 1,150 × 930 (16% of the total simulation slab area), plots **c** and **d** show a section of 1,150 × 575 (10% of the total simulation slab area).

Crack speed and energy flow

We show by molecular-dynamics simulations that a localized, small hyperelastic region around the crack tip can have significant effects on the dynamics of crack propagation.

In all simulations, the slab is statically loaded with 0.32% strain in mode I. The strain energy density far ahead of the crack tip is given by $S = 0.5\varepsilon_{xx}^2 l_x E/(1-\nu^2)$, where E is the Young's modulus at small strain. The linear elastic expression of strain energy density is valid because material far ahead of the crack is strained always below the onset threshold of the bilinear law, that is, it remains in the linear elastic regime of material response. The strain and strain energy density both vanish far behind the crack. For a unit distance of crack propagation, a strip of material with energy density S ahead of the crack is replaced by an identical strip with zero strain energy behind the crack. According to the linear elastodynamic theory of fracture[1], the crack speed should satisfy the dynamic energy release rate equation $A(v/c_R) = 2\gamma/S$ where the function $A(v/c_R)$ is a universal function of crack velocity for a given material. Assuming that the small-strain elasticity completely governs the dynamics of fracture, the linear theory predicts that crack velocity should depend only on the ratio S/γ. During crack propagation, the energy stored ahead of the crack tip is partly converted by the bond-breaking process into fracture surface energy, and partly dissipated into atomic motion.

In the purely harmonic case, the fracture surface energy γ depends on r_{break} and E. In the biharmonic case, the fracture surface energy depends on r_{break}, r_{on}, E_1 and E_2. Our strategy is to focus on the prediction from linear theory that crack velocity depends only on the ratio S/γ. To achieve this objective, we keep the ratio S/γ constant in all of the simulations. In the harmonic systems, as $S \propto E$ and $\gamma \propto E$ (see Methods section), we choose the parameter r_{break} to be identical in all cases. In the biharmonic systems, we adjust the parameter r_{break}, at given values of r_{on}, E_1 and E_2, to always keep S/γ constant.

We choose $r_{break} = 1.17$ for the harmonic systems. The failure strain at the crack tip can reach a magnitude of several per cent, which is comparable to many 'real materials'. In the harmonic systems (with Young's modulus equal to E_1 or E_2), the crack achieves the same propagation velocity of around 80% of the Rayleigh wave speed. This is consistent with the linear theory.

For the biharmonic systems, we choose $r_{on} = 1.1275$ and $r_{break} = 1.1558$ in the stiffening system and $r_{break} = 1.1919$ in the softening system to keep S/γ constant. In contrast to the linear theory prediction, we find that the crack propagation velocity is about 20% larger in the stiffening system and 30% smaller in the softening system. These deviations cannot be explained by the linear theory. The fact that we change the large-strain elasticity while keeping the small-strain elasticity constant indicates that hyperelasticity is affecting crack dynamics.

A geometric criterion based on the principal strain is used to characterize the area with hyperelastic material response close to the crack tip. The region occupied by atoms having a local maximum principal strain $\epsilon_1 > (r_{on}-r_1)/r_1$ defines the hyperelastic area A. Figure 2a shows the hyperelastic area in the case of a stiffening material, and Fig. 2b shows the hyperelastic area in the case of an elastically softening material, indicating that the hyperelastic effect is highly localized to the crack tip (these pictures show a portion of the simulation slab near the crack tip). However, the effect of hyperelasticity on crack velocity is significant, independent of the slab size.

A measure for the direction and magnitude of energy flow in the vicinity of the crack tip is the dynamic Poynting vector[1,26]. The magnitude of the dynamic Poynting vector, $P = \sqrt{P_1^2 + P_2^2}$, may be identified as a measure for the local energy flow. A measure for the enhancement or reduction of energy flow is obtained by subtracting

Table 1 **Change of energy flow towards the crack tip**

	Change of net energy flow to crack tip	Change of energy flow towards crack tip	Change of energy flow away from crack tip	Change of limiting speed
Stiffening	+19%	+20%	+25%	+20%
Softening	−32%	−32%	−35%	−30%

The table summarizes change of net energy flow, change of energy flow towards the crack tip and change of energy flow away from the crack tip, in comparison to the harmonic system.

the magnitude of the dynamic Poynting vector in the harmonic case from that in the biharmonic case at every point in the slab, $\Delta P = P = P_{\mathrm{biharm}} - P_{\mathrm{harm}}$. If the difference is negative, energy flow is reduced, and if the difference is positive, energy flow is enhanced. The steady-state fields are averaged over space as well as time to obtain good statistics.

Figure 2 shows the energy flow enhancement and reduction in the vicinity of the crack tip for the elastically stiffening bilinear system (Fig. 2c) and for the elastically softening system (Fig. 2d). In each plot, the local hyperelastic zone is indicated by a dotted line. The energy flow in the vicinity of the crack tip is enhanced in the bilinear stiffening case and reduced in the softening case. In these plots, we also indicate the direction of energy flow with arrows and note that in the softening case, the energy flow ahead of the crack almost vanishes. The plots show that the local hyperelastic effect leads to an enhancement (stiffening system) or reduction (softening system) in energy flow. The small hyperelastic regions enhance the energy flow around the crack tip. The higher crack velocity in the stiffening system and the lower velocity in the softening system are due to enhancement or reduction of the energy flow in the vicinity of the crack tip.

Table 1 summarizes change of net energy flow, as well as change of energy flow towards and away from the crack tip, in comparison to the harmonic system. The results quantify those depicted in Fig. 2c and d and show that the net energy flow as well as the flow of energy towards and away from the crack tip are all enhanced in the stiffening case, and reduced in the softening case. The integral of energy flux, or path-independent dynamic *J*-integral, around the crack tip increases by 19% in comparison with the harmonic case for the stiffening system, while decreasing by 32% for the softening system.

How fast can cracks propagate?

We have learned that a local hyperelastic zone around the crack tip can have significant effect on the velocity of the crack. For a mode I tensile crack, linear theory predicts that the energy release rate vanishes for all velocities in excess of the Rayleigh wave speed[1–3], implying that a mode I crack cannot move faster than the Rayleigh wave speed. This prediction is indeed confirmed in systems with the harmonic potential where crack velocity approaches the Rayleigh wave speed independently of the slab size, provided that the applied strain is larger than 1.08% and the slab width is sufficiently large ($l_x > 1{,}000$). The systems are loaded dynamically in this case. Our strain levels are about ten times lower than in many other studies[24].

We consider hyperelastic effect of different strengths by using a biharmonic potential with different onset strains governed by the parameter r_{on}. The parameter r_{on} governs the onset strain of the hyperelastic effect $\epsilon_{\mathrm{on}} = (r_{\mathrm{on}} - r_1)/r_1$. The simulations reveal crack propagation at super-Rayleigh velocities in steady-state with a local stiffening zone around the crack tip. Figure 3a plots the crack velocity as a function of the hyperelasticity onset strain ϵ_{on}. The crack speeds shown in Fig. 3 are determined during steady-state propagation. We observe that the earlier the hyperelastic effect is turned on, the larger the limiting velocity. Measuring the hyperelastic area using the principal strain criterion, we find that the area grows as ϵ_{on} becomes smaller. A correlation of the square root of the hyperelastic area with the achieved limiting speed of the crack is shown in Fig. 3a. In Fig. 3b, we depict the shape of the hyperelastic area near the crack tip for different choices of ϵ_{on}. The shape and size of the hyperelastic region is found to be independent of the slab width l_x. In all cases, the hyperelastic area remains confined to the crack tip and does not extend to the boundary of the simulation. Figure 3 shows that the hyperelastic effect is very sensitive to the potential parameter and the extension of the local hyperelastic zone.

Mode I cracks can travel at steady-state intersonic velocities if there exists a locally stiffening hyperelastic zone. For example, when the large-strain spring constant is chosen to be $k_2 = 4k_1$, with $r_{\mathrm{on}} = 1.1375$ and $r_{\mathrm{break}} = 1.1483$ (that is, 'stronger' stiffening and thus larger local wave velocity than before), the mode I crack propagates 21% faster than the Rayleigh speed of the soft material, and becomes intersonic, as shown by the Mach cone of shear wave front depicted in Fig. 4a.

We have also simulated a shear-dominated mode II crack using the biharmonic stiffening potential. We define $r_{\mathrm{break}} = 1.17$, and r_{on} is chosen slightly below r_{break} to keep the hyperelastic region small. The dynamic loading is stopped soon after the daughter crack is nucleated[25,27,28]. The result is shown in Fig. 4b. The daughter crack nucleated from the mother crack propagates supersonically through the material, although the hyperelastic zone remains localized to the crack tip region. Supersonic mode II crack propagation has been observed previously[23,25] using an anharmonic stiffening potential. However, a clearly defined hyperelastic zone could not be specified in those simulations. Our result proves that a local hyperelastic stiffening effect at the crack tip causes supersonic crack propagation, in contrast to the linear continuum theory.

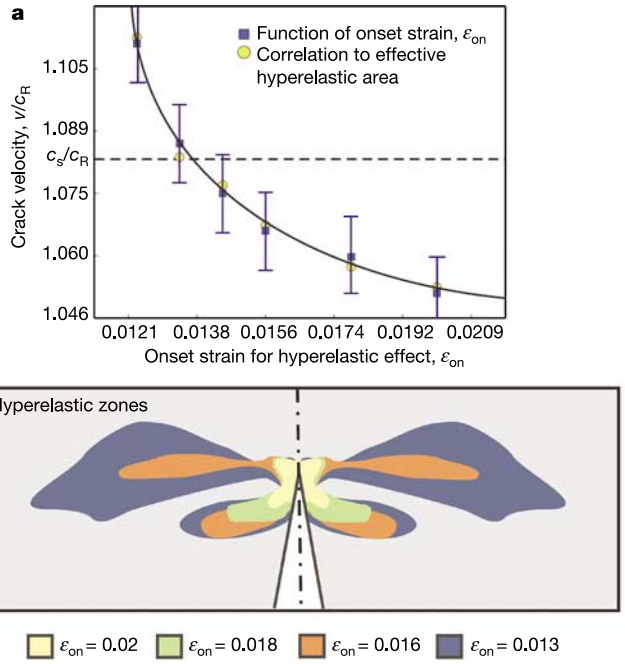

Figure 3 Change of crack speed with the onset strain of hyperelasticity. The crack speed as a function of the onset strain of hyperelasticity ϵ_{on}, as well as a correlation of the crack speed with the square root of the hyperelastic area is shown in **a**. In **b**, the shape of the hyperelastic zone near the crack tip is shown for different onset strains, indicating that the hyperelastic area remains confined to the vicinity of the crack tip. **b**, A section of 1,650 × 570 (9% of the total simulation slab area).

The observation of super-Rayleigh and intersonic mode I cracks, as well as supersonic mode II cracks, clearly contradicts the prediction by the classical theories of fracture.

Characteristic energy length scale

The problem of a super-Rayleigh mode I crack in an elastically stiffening material is somewhat analogous to Broberg's[29] problem of a mode I crack propagating in a stiff elastic strip embedded in a soft matrix. The geometry of this problem is shown in Fig. 5a. Broberg[29] has shown that, when such a crack propagates supersonically with respect to the wave speeds of the surrounding matrix, the energy release rate can be expressed in the form

$$G = \frac{\sigma^2 h}{E} f(\nu, c_1, c_2) \quad (1)$$

where σ is the applied stress, h is the half-width of the stiff layer and f is a non-dimensional function of crack velocity and wave speeds in the strip and the surrounding matrix (c_1, c_2). The dynamic Griffith energy balance requires $G = 2\gamma$, indicating that crack propagation velocity is a function of the ratio h/χ where $\chi \propto \gamma E/\sigma^2$ can be defined as a characteristic length scale for local energy flux. By dimensional analysis, the energy release rate of our hyperelastic stiffening material is expected to have similar features except that Broberg's strip width h should be replaced by a characteristic size of the hyperelastic region r_H. Therefore, we introduce the concept of a characteristic length

$$\chi = \beta \frac{\gamma E}{\sigma^2} \quad (2)$$

for local energy flux near a crack tip. The coefficient β may depend on the ratio between hyperelastic and linear elastic properties. We have simulated the Broberg problem and found that the mode I crack speed reaches the local Rayleigh wave speed as soon as h/χ reaches unity. Numerous simulations verify that the scaling law in equation (2) holds when γ, E and σ is changed independently. The results are shown in Fig. 5b. From the simulations, we estimate numerically $\beta \approx 87$ and $\chi \approx 750$.

The existence of a characteristic length for local energy flux near the crack tip has not been discussed in the literature and plays the central role in understanding the effect of hyperelasticity. Under a particular experimental or simulation condition, the relative importance of hyperelasticity is determined by the ratio r_H/χ. For small r_H/χ, the crack dynamics is dominated by the global linear elastic properties because much of the energy transport necessary to sustain crack motion occurs in the linear elastic region. However, when r_H/χ approaches unity, as is the case in some of our molecular-dynamics simulations, the dynamics of the crack is dominated by local elastic properties because the energy transport required for crack motion occurs within the hyperelastic region.

The concept of energy characteristic length χ immediately explains how the classical barrier for transport of energy over large distances can be undone by rapid transport near the tip.

Discussion and conclusions

We have shown that local hyperelasticity has a significant effect on the dynamics of brittle crack speeds and have discovered a characteristic length associated with energy transport near a crack tip. The assumption of linear elasticity fails if there is a hyperelastic zone in the vicinity of the crack tip comparable to the energy characteristic length. Therefore, we conclude that hyperelasticity is crucial for understanding and predicting the dynamics of brittle fracture. Our simulations prove that even if the hyperelastic zone extends only a small area around the crack tip, there may be crucial effects on the limiting speed and the energy flow towards the crack tip, as illustrated in Fig. 3. If there is a local softening effect, we find that the limiting crack speed is lower than in the case of harmonic solid.

Our study has shown that hyperelasticity dominates the energy transport process when the hyperelastic zone size becomes comparable to the characteristic length $\chi \propto \gamma E/\sigma^2$. Under normal experimental conditions, the magnitude of stress may be one or

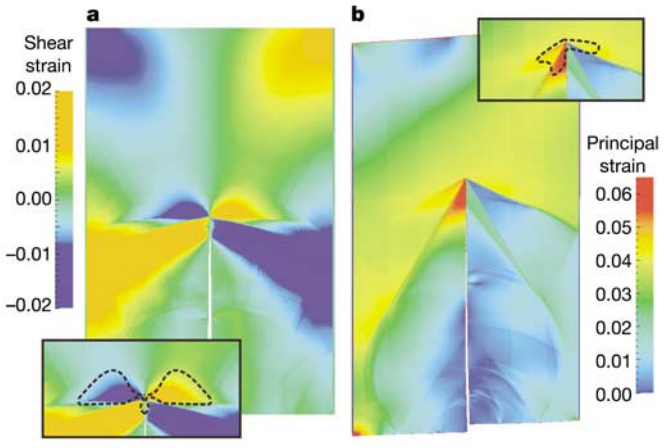

Figure 4 Intersonic mode I crack motion and supersonic mode II crack motion. **a**, The shear strain field in a section of the slab during intersonic mode I crack propagation. The Mach cone is associated with the shear wave speed. The hyperelastic zones are indicated in the insets by dotted lines. **b**, The principal strain field of a crack propagating at a supersonic velocity in mode II. The two Mach cones associated with shear wave and longitudinal wave can clearly be recognized. These plots illustrate that cracks can move with super-Rayleigh speeds under mode I loading and supersonic speeds under mode II loading. The classical theory of fracture cannot explain these results.

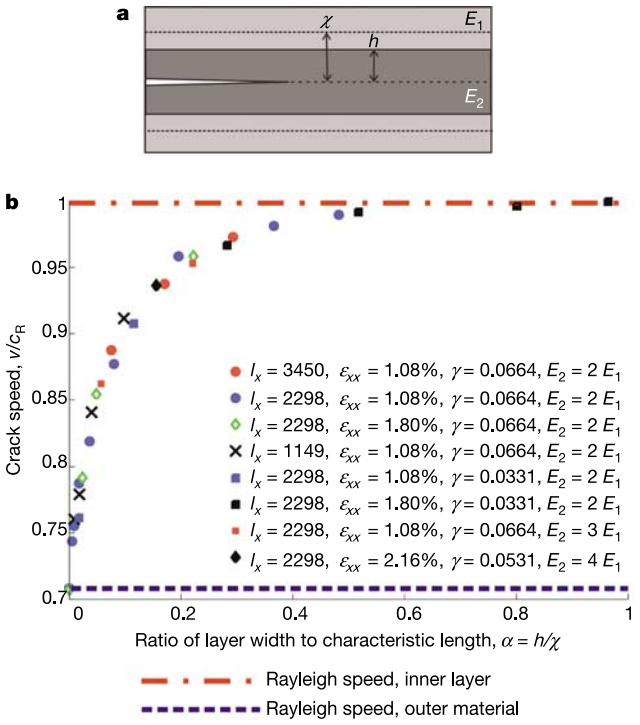

Figure 5 Scaling law for the characteristic length associated with energy transport near the crack tip. **a**, Broberg's problem. **b**, The simulation results of crack velocity versus the half-width h of Broberg's stiff layer normalized by the characteristic $\chi = \beta\gamma E/\sigma^2$. The simulation results from a variety of different simulation cases (for example, variation of surface energy, Young's modulus, loading) confirm the scaling law for the characteristic length of energy transport near the crack tip. Once h reaches the characteristic length, the crack velocity reaches the Rayleigh velocity of the inner layer.

two orders of magnitude smaller than that under molecular-dynamics simulations. In such cases, the characteristic length χ is relatively large and the effect of hyperelasticity on effective velocity of energy transport is relatively small. However, χ decreases with the square of the applied stress. At about 1% of elastic strain as in our simulations, this zone is already on the order of a few hundred atomic spacing and significant hyperelastic effects are observed.

Our simulations indicate that the universal function $A(v/c_R)$ in the classical theory of dynamic fracture is no longer valid once the hyperelastic zone size r_H becomes comparable to the energy characteristic length χ. Linear elastic fracture mechanics predicts that the energy release rate of a mode I crack vanishes for all velocities in excess of the Rayleigh wave speed. However, this is only true if $r_H/\chi \ll 1$. A hyperelastic theory of dynamic fracture should incorporate this ratio into the universal function so that the function should be generalized as $A(v/c_R, r_H/\chi)$. The local hyperelastic zone changes not only the near-tip stress field within the hyperelastic region, but also induces a finite change in the integral of energy flux around the crack tip. We find that the dynamic J-integral around a super-Rayleigh (Fig. 3) mode I crack is still path-independent but no longer vanishes in the presence of hyperelasticity. Similarly, the supersonic mode II crack motion (Fig. 4b) can only be understood from the point of view of hyperelasticity. A single set of global wave speeds is not capable of capturing all phenomena observed in dynamic fracture.

We believe that the length scale χ, heretofore missing in the existing theories of dynamic fracture, will prove to be helpful in forming a comprehensive picture of crack dynamics. In most engineering and geological applications, typical values of stress are much smaller than those in molecular-dynamics simulations. In such cases, the ratio r_H/χ is small and the effective speed of energy transport is close to predictions by linear elastic theory. However, the effect of hyperelasticity will be important for nanoscale materials, such as highly strained thin films or nanostructured materials, as well as high-speed impact phenomena. □

Methods

Molecular dynamics simulation procedure

Our simulation tool is classical molecular dynamics[23,30]. Molecular dynamics predicts the motion of a large number of atoms governed by their mutual interatomic interaction, and it requires numerical integration of the equations of motion, usually via a Verlet algorithm with time step $\Delta t = 0.0036$ (refs 23, 30) (in reduced time unit). The slab size is chosen large enough such that waves reflected from the boundary do not interfere with the propagating crack. We establish a linear velocity gradient before simulation to avoid shock wave generation from the boundaries. To strain the system, we use two approaches. The first is using a constant strain rate applied over a loading time t, by displacing the outermost rows of atoms. After the loading time, the boundaries are kept fixed. In the second method, we strain the system before simulation in the loading direction, and keep the boundary fixed during simulation. In either way, the crack starts to move once a critical strain is applied. It can be shown that the stress intensity factor remains constant in a strip geometry inside a region of $3/4l_x < a < (l_y - 3/4l_x)$ (refs 24, 31). This ensures that the crack achieves a steady-state during propagation through the slab. The slab is initialized at zero temperature before simulation.

Slab geometry and typical length scales

The length l_y is several times larger than l_x, with the ratio l_y/l_x ranging from two to five. The slab width l_x considered ranges from 1,150 (smallest) up to 4,597 (largest, corresponding to micrometre length scale in physical dimensions). The largest model contains over 70 million atoms. All quantities in this paper are given in reduced units. The condition for small-scale yielding is satisfied in all cases (with harmonic, stiffening and softening potentials), because breaking of atomic bonds occurs over a region involving only a few atoms along the weak layer (that is, a very small fracture process zone). There is no dislocation process and the system is perfectly brittle. The slab is loaded with a maximum of a few per cent strain, according to the crack loading mode. The loading is significantly lower than other studies[24]. A slit of length $a = 200$ is cut midway through the slab as an initial, atomically sharp crack.

Interatomic potential

The interatomic potential is defined as

$$\phi(r) = \begin{cases} 1/2k_1(r - r_1)^2 & \text{if } r < r_{on} \\ a_2 + 1/2k_2(r - r_2)^2 & \text{if } r \geq r_{on} \end{cases} \quad (3)$$

The other parameters of the potential are determined to be $a_2 = 1/2k_1(r_{on} - r_1)^2 - 1/2k_2(r_{on} - r_2)^2$, and $r_2 = 1/2(r_{on} + r_1)$ from continuation conditions. For a harmonic two-dimensional elastic sheet of atoms, Young's modulus is given by $E = \frac{2}{\sqrt{3}}k_1$, and the shear modulus is $\mu = \frac{\sqrt{3}}{4}k_1$ (see for example, ref. 16).

Crack tip velocity measurements

Accurate determination of crack tip velocity is important because we need to be able to measure even the smallest changes in the propagation speed. The crack tip position is determined by finding the surface atom with maximum y position in the interior of a search region inside the slab. This quantity is averaged over a small time interval to eliminate very-high-frequency fluctuations. To obtain the steady-state velocity of the crack, the measurements are taken within a region of constant stress intensity factor[24,31]. In addition to checking the velocity history, steady-state is verified by path-independency of the energy flux integral[1].

Fracture surface energy

The fracture surface energy γ is defined as the energy necessary to break atomic bonds per unit crack advance, and is given by

$$\gamma = \frac{E(r_{break} - r_1)^2}{2r_1} \quad (4)$$

for the purely harmonic potential and

$$\gamma = \frac{2a_2 + k_2(r_2 - r_{break})^2}{\sqrt{3}r_1} = \frac{E_1(r_{on} - r_1)^2 - E_2((r_{on} - r_2)^2 - (r_2 - r_{break})^2)}{2r_1} \quad (5)$$

for the biharmonic potential (if $r_{break} > r_{on}$), where E_1 is the Young's modulus associated with small deformations, and E_2 is the Young's modulus associated with large deformations.

Atomic strain

We define the left Cauchy–Green strain tensor of an atom l (ref. 32)

$$b_{ij} = \left\{ \frac{1}{3r_1^2} \sum_{k=1}^{N} [(x_i^l - x_i^k)(x_j^l - x_j^k)] \right\} \quad (6)$$

with $N = 6$ nearest neighbours. Unlike the virial stress, the virial strain is valid instantaneously in space and time. The maximum principal strain b_1 is obtained by diagonalization of the strain tensor b_{ij}. The maximum principal engineering strain is then given by $\varepsilon_1 = \sqrt{b_1} - 1$.

Energy flow analysis

Under steady-state conditions, the net energy flow to the crack tip is defined by an integration of the product of dynamic Poynting vector with surface normal n_j over a contour $\partial\Omega$ surrounding the crack tip, (the contour could be selected as a circle around the crack tip)[1]

$$F_N(\partial\Omega) = \int_{\partial\Omega} \{\sigma_{ij} n_j \dot{u}_i + (U + T)v n_1\} \cdot d\Omega \delta_i \quad (7)$$

Here, the dynamic Poynting vector $P_j = \sigma_{ij}\dot{u}_i + (U + T)v\delta_{1j}$ measures the local energy flow, with stress σ_{ij}, particle velocity $\dot{u}_i$, potential energy density U, kinetic energy density T, and crack propagation speed v.

Computing techniques and supercomputing centre

A FORTRAN molecular-dynamics code parallelized with MPI is used for the simulations. We use the IBM XL FORTRAN compiler for AIX for compilation of the source code. The simulations are carried out on IBM Power 4 Regatta nodes in the Max Planck Society Supercomputer Centre in Munich.

Received 17 April; accepted 19 September 2003; doi:10.1038/nature02096.

1. Freund, L. B. *Dynamic Fracture Mechanics* 2nd edn (Cambridge Univ. Press, Cambridge, UK, 1998).
2. Broberg, B. *Cracks and Fracture* (Academic, San Diego, 1999).
3. Slepyan, L. I. *Models and Phenomena in Fracture Mechanics* (Springer, Berlin, 2002).
4. Fineberg, J., Gross, S. P., Marder, M. & Swinney, H. L. Instability in dynamic fracture. *Phys. Rev. Lett.* **67,** 141–144 (1991).
5. Ravi-Chandar, K. Dynamic fracture of nominally brittle materials. *Int. J. Fract.* **90,** 83–102 (1998).
6. Abraham, F. F., Brodbeck, D., Rudge, W. E. & Xu, X. Instability of fracture—a computer-simulation investigation. *Phys. Rev. Lett.* **73,** 272–275 (1994).
7. Abraham, F. F., Brodbeck, D. & Rudge, W. E. A molecular-dynamics investigation of rapid fracture mechanics. *J. Mech. Phys. Solids* **45,** 1595–1619 (1997).
8. Falk, M. L., Needleman, A. & Rice, J. R. A critical evaluation of cohesive zone models of dynamic fracture. *J. Phys. IV France* **11,** 43–50 (2001).
9. Washabaugh, P. D. & Knauss, W. G. A reconcilation of dynamic crack velocity and Rayleigh-wave speed in isotropic brittle solids. *Int. J. Fract.* **65,** 97–114 (1994).
10. Sharon, E. & Fineberg, J. Confirming the continuum theory of dynamic brittle fracture for fast cracks. *Nature* **397,** 333 (1999).
11. Field, J. E. Brittle fracture—its study and application. *Contemp. Phys.* **12,** 1–31 (1971).
12. Cramer, T., Wanner, A. & Gumbsch, P. Energy dissipation and path instabilities in dynamic fracture of silicon single crystals. *Phys. Rev. Lett.* **85,** 788–791 (2000).
13. Hauch, J. A. & Marder, M. P. Energy balance in dynamic fracture, investigated by a potential drop technique. *Int. J. Fract.* **90** (1–2), 133–151 (1998).
14. Hauch, J. A., Holland, D., Marder, M. P. & Swinney, H. L. Dynamic fracture in single crystal silicon. *Phys. Rev. Lett.* **82,** 3823–3826 (1999).
15. Hull, D. & Beardmore, P. Velocity of propagation of cleavage cracks in Tungsten. *Int. J. Fract. Mech.* **2,** 468–488 (1966).

16. Gao, H. A theory of local limiting speed in dynamic fracture. *J. Mech. Phys. Solids* **44,** 1453–1474 (1996).
17. Gao, H. Elastic eaves in a hyperelastic solid near its plane-strain equibiaxial cohesive limit. *Phil. Mag. Lett.* **76,** 307–314 (1997).
18. Abraham, F. F. Dynamics of brittle fracture with variable elasticity. *Phys. Rev. Lett.* **77,** 272–275 (1996).
19. Abraham, F. F.. *et al.* Instability dynamics in three-dimensional fracture: An atomistic simulation. *J. Mech. Phys. Solids* **45,** 1461–1471 (1997).
20. Rountree, C. L. *et al.* Atomistic aspects of crack propagation in brittle materials: Multimillion atom molecular-dynamics simulations. *Annu. Rev. Mater. Res.* **32,** 377–400 (2002).
21. Zhou, S. J., Lomdahl, P. S., Thomson, R. & Holian, B. L. Dynamic crack processes via molecular-dynamics. *Phys. Rev. Lett.* **76,** 2318–2321 (1996).
22. Heizler, S. I., Kessler, D. A. & Levine, H. Mode I fracture in a nonlinear lattice with viscoelastic forces. *Phys. Rev. E* **6,** 016126 (2002).
23. Abraham, F. F *et al.* Simulating materials failure by using up to one billion atoms and the world's fastest computer: Brittle fracture. *Proc. Natl Acad. Sci. USA* **99,** 5777–5782 (2002).
24. Swadener, J. G., Baskes, M. I. & Nastasi, M. Molecular dynamics simulation of brittle fracture in silicon. *Phys. Rev. Lett.* **89,** 085503 (2002).
25. Abraham, F. F. The atomic dynamics of fracture. *J. Mech. Phys. Solids* **49,** 2095–2111 (2001).
26. Fratini, S., Pla, O., Gonzalez, P., Guinea, F. & Louis, E. Energy radiation of moving cracks. *Phys. Rev. B* **66,** 104104 (2002).
27. Abraham, F. F. & Gao, H. How fast can cracks propagate? *Phys. Rev. Lett.* **84,** 3113–3116 (2000).
28. Rosakis, A. J. Intersonic shear cracks and fault ruptures. *Adv. Phys.* **51,** 1189–1257 (2002).
29. Broberg, K. B. Dynamic crack propagation in a layer. *Int. J. Sol. Struct.* **32**(6–7), 883–896 (1995).
30. Allen, M. & Tildesley, D. *Computer Simulation of Liquids* (Oxford Univ. Press, 1989).
31. Knauss, W. G. Stresses in an infinite strip containing a semi-infinite crack. *J. Appl. Mech.* **33,** 356–362 (1966).
32. Zimmermann, J. *Continuum and Atomistic Modeling of Dislocation Nucleation at Crystal Surface Ledges* PhD thesis, Stanford Univ. (1999).

Acknowledgements F.F.A. acknowledges the generous support provided by the Humboldt Research Award for Senior US Scientists.

Competing interests statement The authors declare that they have no competing financial interests.

Correspondence and requests for materials should be addressed to H.G. (hjgao@mf.mpg.de).